

# Ram pressure on simulated low-mass Local Group galaxies

Jenna Samuel<sup>1\*</sup><sup>†</sup>, Bhavya Pardasani<sup>2</sup>, Michael Boylan-Kolchin<sup>1</sup>, Andrew Wetzel<sup>3</sup>,

<sup>1</sup>Department of Astronomy, The University of Texas at Austin, 2515 Speedway, Stop C1400, Austin, TX 78712, USA

<sup>2</sup>Department of Astronomy, University of Illinois at Urbana-Champaign, 1002 W Green St, Urbana, IL 61801, USA

<sup>3</sup>Department of Physics and Astronomy, University of California, Davis, CA 95616, USA

Accepted XXX. Received YYY; in original form ZZZ

## ABSTRACT

Low-mass galaxies are highly susceptible to external environmental effects that can quenching star formation. We explore the role of ram pressure in the regulation of gas content and quenching of low-mass galaxies ( $M_* = 10^{5-10} M_\odot$ ) within 2 Mpc of Milky Way (MW) mass galaxies using the FIRE-2 simulations. Ram pressure is highly variable across different environments, within a MW-mass halo, and over time. Galaxies in low-mass groups ( $M_{*,\text{host}} \approx 10^{7-10} M_\odot$ ) outside of a MW-mass halo experience significant ram pressure similar to MW satellites, helping to explain effective quenching via group pre-processing. The strength of maximum ram pressure experienced before quenching is insufficient on its own to separate the populations of quiescent and star-forming galaxies, but the impulsiveness of the maximum ram pressure, or the maximum ram pressure scaled to the integrated ram pressure, strongly correlates with whether a galaxy is quiescent or star-forming. Ram pressure rises sharply with decreasing distance to a MW-mass host, and at fixed distance more recent pericenter passages are typically associated with higher ram pressure because of greater density of the inner host circumgalactic medium (CGM) at late times. The host CGM density near paired Local Group-like hosts is larger at small angles ( $\lesssim 30^\circ$ ) off the host galaxy disk. The quiescent fraction of satellite galaxies and the ram pressure within these low-latitude regions is slightly larger around the paired hosts compared to the isolated hosts.

**Key words:** galaxies: evolution – galaxies: Local Group – methods: numerical

## 1 INTRODUCTION

Star formation in low-mass galaxies ( $M_* \lesssim 10^9 M_\odot$ ) can be efficiently quenched by internal processes and interactions with the environment because their shallow gravitational potentials cannot provide sufficient gravitational restoring force to retain the gas that fuels star formation. Internally, galaxies experience feedback from cycles of energetic outbursts coming from stars and accreting supermassive black holes. Externally, galaxies interact with the environment gravitationally, hydrodynamically, and radiatively. In particular, galaxies can efficiently lose gas and quench through ram pressure stripping due to their motion through an ambient gas medium ( $P_{\text{ram}} \approx \rho v^2$ ) (e.g., Gunn & Gott 1972; McCarthy et al. 2008; Grcevich & Putman 2009). Ram pressure stripping is often identified in massive group and cluster environments by the presence of so-called jellyfish galaxies with neutral hydrogen (HI) tails extending opposite their direction of motion.

Ram pressure stripping is typically thought to proceed outside-in, whereby gas at the outskirts of a halo is easier to remove because of lower gravitational restoring forces (e.g., McCarthy et al. 2008). Recent work has also shown that ram pressure can remove gas from the outskirts of a galaxy while compressing the inner dense gas and causing further star formation (e.g., Tonnesen & Bryan 2009;

Genina et al. 2019; Wright et al. 2019; Hausammann et al. 2019; Di Cintio et al. 2021). However, Fillingham et al. (2015) showed that in order to match the observed quiescent fraction of satellite galaxies in the Local Group (LG), the satellites must have encountered dense, clumpy gas causing high ram pressure. This paints a picture of two modes of ram pressure that affect a galaxy’s star formation: smooth ram pressure that slowly removes gas and cuts off fresh gas accretion, and bursty ram pressure that completely strips a galaxy of its ISM and rapidly quenches its star formation.

Studies of ram pressure often focus on the densest environments like massive galaxy clusters and groups, where ram pressure effects are the most obvious. However, recent studies have also found evidence for ram pressure effects in less dense environments. For example, the collapse of large scale structures like sheets and filaments can shock heat the intergalactic medium (IGM) at early times ( $z = 2 - 5$ ) and quench otherwise isolated galaxies that interact with the shock front (Pasha et al. 2022). Even LG galaxies that are far away from the MW/M31 seem to be experiencing ram pressure/environmental quenching: WLM (930 and 830 kpc from the MW and M31, respectively) has trailing clouds of HI gas indicative of ram pressure stripping (Yang et al. 2022) and low-mass galaxies from the FIRE simulations show evidence for environmental quenching out to  $\approx 1$  Mpc from MW-mass hosts (Samuel et al. 2022).

In the Local Group (LG), the gas-poor nature of most low-mass galaxies close to the Milky Way (MW) and Andromeda (M31) compared to more isolated galaxies at similar mass imply that their gas

\* E-mail: jenna.samuel@austin.utexas.edu

† NSF Astronomy and Astrophysics Postdoctoral Fellow

is efficiently removed by environmental processes like ram pressure (e.g., Putman et al. 2021). The short quenching timescales estimated for observed LG galaxies and those in simulations suggest that a rapid process like ram pressure stripping from a clumpy circumgalactic medium (CGM) may be responsible for removing their gas (e.g., Fillingham et al. 2015; Wetzel et al. 2015; Samuel et al. 2022).

Ram pressure in the LG has been examined using simulations like Figuring Out Gas in GalaxIEs (FOGGIE), that are specifically designed to enforce uniform resolution throughout the CGM of MW-mass hosts. Using FOGGIE, Simons et al. (2020) find that ram pressure is stochastic (i.e., it varies significantly on short timescales) when they calculate ram pressure in the immediate path of a satellite galaxy versus using a spherically averaged density profile around a host.

In this work, we seek to understand the conditions necessary for ram pressure to remove the ISM from and thus quench low-mass galaxies. In Section 2, we describe the simulations and how we measure ram pressure histories for each galaxy. In Section 3, we present ram pressure histories (3.2), describe the ram pressure conditions necessary to quench galaxies (3.3), characterize the strength of ram pressure on MW satellites at pericenter passage (3.4), and examine effects of angular anisotropy in the host CGM on ram pressure in the inner halo and the quiescent fraction of satellites (3.5). In Section 4, we summarize our findings and discuss their implications for quenching via ram pressure in the Local Group and beyond.

## 2 SIMULATIONS

We analyze low-mass galaxies around 14 MW/M31-mass host galaxies from the FIRE simulation project<sup>1</sup>. Eight host galaxies are isolated (Latte) and six are in LG-like pairs (ELVIS on FIRE) (Wetzel et al. 2016). The six paired hosts and one isolated host were simulated with  $m_{\text{baryon,ini}} = 3500 - 4200 \text{ M}_\odot$  ( $m_{\text{dm}} \approx 2 \times 10^4 \text{ M}_\odot$ ), and the other seven isolated hosts were simulated with  $m_{\text{baryon,ini}} = 7100 \text{ M}_\odot$  ( $m_{\text{dm}} = 3.5 \times 10^4 \text{ M}_\odot$ ). We generated cosmological zoom-in initial conditions using MUSIC (Hahn & Abel 2011) with flat  $\Lambda$ CDM cosmologies that are broadly consistent with Planck Collaboration et al. (2018), see Samuel et al. (2022) for more details.

We ran the simulations with the FIRE-2 implementations of fluid dynamics, star formation, and stellar feedback (Hopkins et al. 2018b). FIRE uses the GIZMO Lagrangian meshless finite-mass (MFM) hydrodynamics solver (Hopkins 2015) and gravitational forces are solved using an upgraded version of the  $N$ -body GADGET-3 Tree-PM solver (Springel 2005). GIZMO enables adaptive hydrodynamic gas smoothing based on the local density of gas cells while still conserving mass, energy, and momentum to machine accuracy.

FIRE-2's subgrid model for gas implements a metallicity-dependent treatment of radiative heating and cooling over  $10 - 10^{10} \text{ K}$  (Hopkins et al. 2018b), a cosmic ultraviolet background ( $z_{\text{reion}} \sim 10$ ) (Faucher-Giguère et al. 2009), and turbulent diffusion of metals (Hopkins 2016; Su et al. 2017; Escala et al. 2018). Star formation in FIRE-2 occurs in gas that is self-gravitating, Jeans-unstable, cold ( $T < 10^4 \text{ K}$ ), dense ( $n > 1000 \text{ cm}^{-3}$ ), and molecular (Krumholz & Gnedin 2011). Several stellar-feedback processes are also included in FIRE-2 via subgrid models, including Ia supernovae, mass loss, photoionization, photoelectric heating, and radiation pressure. Supernovae are individually time-resolved and the FIRE-2 algorithm

for coupling mechanical feedback to the surrounding gas manifestly conserves mass, energy, and momentum (Hopkins et al. 2018a).

These simulations reproduce key elements of the LG satellite population such as the stellar mass function, radial distance distribution, star formation histories, and aspects of satellite planes (Wetzel et al. 2016; Garrison-Kimmel et al. 2019a,b; Samuel et al. 2020, 2021). Of particular relevance to the work in this paper are the star formation histories (SFH) and quiescent fractions of galaxies in the simulations. Garrison-Kimmel et al. (2019b) demonstrated that the low-mass galaxies far from MW-mass hosts in the simulations (non-satellites) have extended SFH, as expected for galaxies that experience weak to no environmental influence from the host. Importantly, the quiescent fraction of satellite galaxies in the simulations rises sharply at  $M_* \lesssim 10^7 \text{ M}_\odot$ , similar to the LG (Samuel et al. 2022).

We assigned gas to satellites following Samuel et al. (2022). Briefly, assigned gas cells must be (1) within  $2R_{*,1/2}$  (stellar half-mass radius) of a subhalo center and (2) within  $2\text{MAX}(V_{\text{max}}, \sigma)$ , where  $V_{\text{max}}$  is the maximum circular velocity and  $\sigma$  is the velocity dispersion of DM particles belonging to the subhalo. We calculate the approximate gas surface density of a galaxy by summing the total mass of gas cells whose centers fall within a spherical aperture of radius  $2R_{*,50}$  and diving by  $\pi R_{*,50}^2$ , neglecting its full 3D structure.

### 2.1 Measuring ram pressure

We calculate the localized ram pressure that each low-mass galaxy experiences using a method similar to that described in Simons et al. (2020). The localized approach to calculating density (as opposed to a spherically-averaged density profile in the host halo) allows us to measure ram pressure at any point within the simulation volume, as opposed to restricting to within the halo of a host galaxy. We measure the ambient gas density and velocity relative to a low-mass galaxy within a cylinder in front of the galaxy at each snapshot. The cylinder's axis points along the direction of the galaxy's velocity. The cylinder's closest face begins at the galaxy's halo radius ( $r_{\text{cyl}} = R_{200}$ ), and its height or length is approximately the distance the galaxy will travel between snapshots ( $h_{\text{cyl}} = v_{\text{sat}} \cdot \Delta t \approx v_{\text{sat}} \cdot 25 \text{ Myr}$ ). The radius of the cylinder is also equal to the galaxy's halo radius. Our geometrical selection of local gas is within a larger volume and is situated farther from a galaxy than that used in Simons et al. (2020), but we find that a galaxy's own ISM can extend well past  $R_{*,1/2}$  at different times owing to stellar feedback and we want to minimize such self-contamination in our ram pressure calculation.

We measure the gas mass within the cylinder by first summing the mass of all gas cells with center positions that fall within the cylinder volume. In some cases, especially in low density environments, the center of a gas cell may not lie within the cylinder, but there is still significant overlap between the gas cell kernel radius ( $h_i$ ) and the cylinder. We compute this overlapping mass contribution by weighting ( $w_i$ ) a gas cell's mass by the integral of its kernel density function within the overlapping region normalized to the full integral of its kernel density function. The kernel density function,  $W(q, h_i)$ , is a cubic spline (see equation H4 in Hopkins 2015) where  $q = r/h_i$  is the distance from the kernel center normalized by the kernel radius. We approximate the integration limits as  $r_1 = d_i - D_{\text{cyl,max}}$  and  $r_2 = h_i$  where  $d_i$  is the distance from the center of the cylinder to the center of an overlapping gas cell,  $D_{\text{cyl,max}} = \text{MAX}(r_{\text{cyl}}, h_{\text{cyl}})$  is the maximum cylinder dimension, and  $h_i$  is the gas cell's kernel radius. This creates a somewhat deformed cylinder boundary due to the spherical distance selection, but it is computationally efficient. We also use the maximum dimension of the cylinder to approximate the

<sup>1</sup> <https://fire.northwestern.edu/>

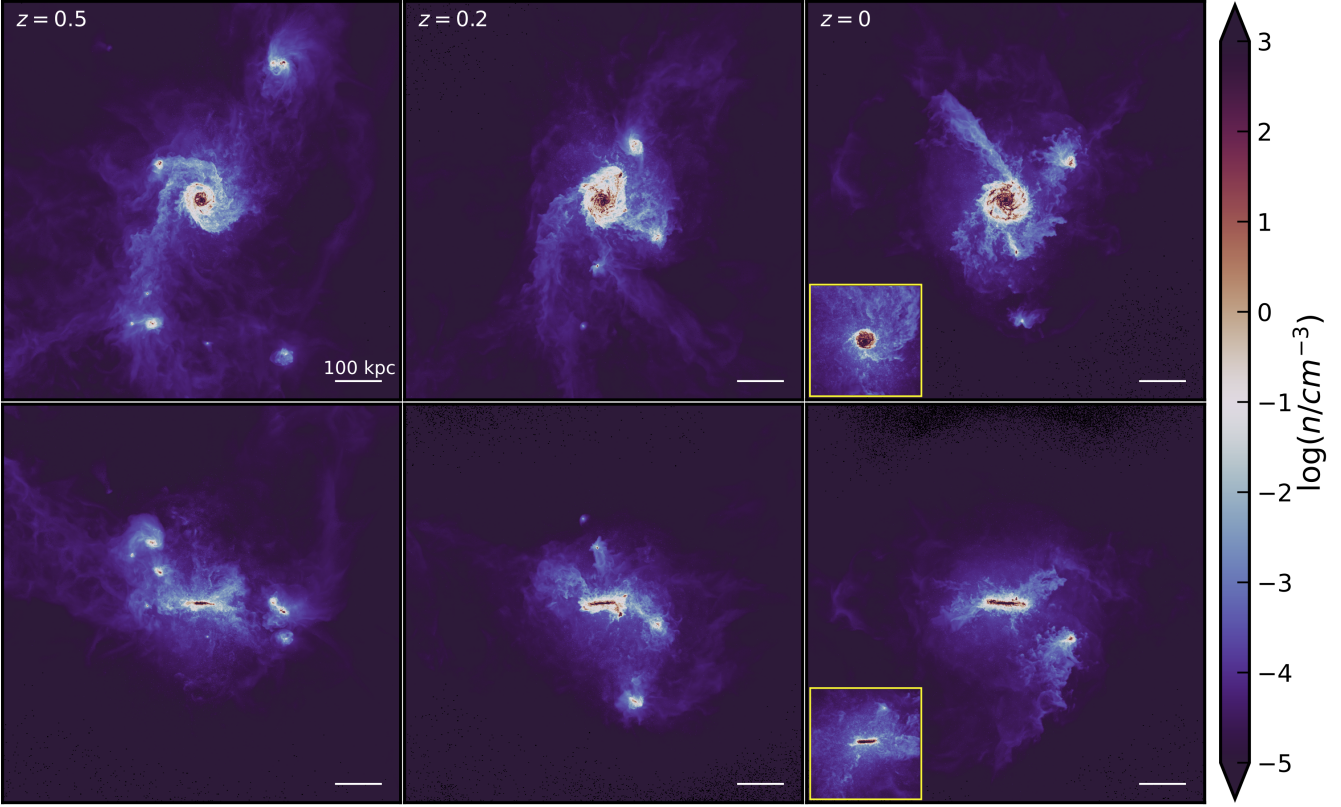


**Figure 1.** Gas density around a paired (LG-like) host (Louise) at three different snapshots every  $\approx 2.5$  Gyr over the last  $\approx 5$  Gyr. The top row is a face-on view of the host and the bottom row is an edge-on view of the host at each snapshot. Gas stripping from satellites is apparent in every panel, and the satellites leave dense gas behind in the host CGM. Insets in the right two panels show the gas disk of an isolated host (m12i) at the same scale, demonstrating that the gas disks of the paired hosts extend farther into the inner halo.

solid angle of the integral  $\Omega_i = 2\pi \left(1 - d_i/\sqrt{d_i^2 + D_{cyl,max}^2}\right)$ . We divide the total gas mass within the cylinder by the cylinder volume to obtain the density of ambient gas contributing to ram pressure.

$$\rho_{gas, ambient} = \frac{1}{V_{cyl}} (M_{gas, inside} + M_{gas, overlap}) \quad (1)$$

$$M_{gas, inside} = \sum_i m_i (|\vec{x}_i - \vec{x}_{cyl}| < D_{cyl,max}) \quad (2)$$

$$M_{gas, overlap} = \sum_i m_i (|\vec{x}_i - \vec{x}_{cyl}| < D_{cyl,max} + h_i) \cdot w_i \quad (3)$$

$$w_i = \frac{\Omega_i \int_{r_1}^{r_2} W(q, h_i) dq}{4\pi \int_0^{h_i} W(q, h_i) dq} \quad (4)$$

We estimate ram pressure using  $P_{ram} \approx \rho v^2$  (e.g., Gunn & Gott 1972), where  $\rho$  is our measured ambient gas mass density and  $v$  is the average velocity of contributing gas cells relative to the galaxy in question (along the cylinder axis). Throughout this paper, we present ram pressure in cgs units as  $g \cdot cm^{-1} \cdot s^{-2}$ . We focus on ram pressure over the last 10 Gyr ( $z \lesssim 1.65$ , 400 snapshots) of the simulations to exclude reionization and high stochasticity in gas density in the early Universe, and to focus on the times when there is a prominent MW host/progenitor (Santistevan et al. 2020).

### 3 RESULTS

#### 3.1 The host CGM

To understand the relationship between the host halo and satellite galaxy quenching, we characterize the density of the host CGM and its effects on satellites. We first quantify CGM density as a function of radius or distance from the host, as we expect the inner halo to be more dense and hence to more efficiently ram pressure strip and quench satellites with close pericenter passages.

Figure 1 shows face-on and edge-on visualizations of gas density around simulated MW-mass host over the last  $\approx 5$  Gyr. We created these images by selecting all gas within a cubical region of side length 950 kpc around the host and coloring each pixel by the maximum density along the line of sight. It is visually apparent that the halo density is higher in the inner regions of the host halo ( $R \lesssim 150$  kpc), and it decreases by 1-2 orders of magnitude at  $R \gtrsim 200$  kpc. However, the CGM is also highly structured with evidence of clumps and filaments throughout, but particularly along the disk plane. The several satellite galaxies and the trails of gas left behind them temporarily enhance the density of the host CGM in small areas by up to three orders of magnitude. The enrichment of the host CGM by stripped satellite gas has previously been noted (Hafen et al. 2019), but here we point out that it likely significantly contributes to the ram pressure experienced by nearby satellite galaxies and hence contributes to quenching their star formation.

We have chosen to visualize this particular host halo (Louise) in Figure 1 because it is one of the paired LG-like hosts, which have larger gas disks and exhibit enhanced gas density in the plane of

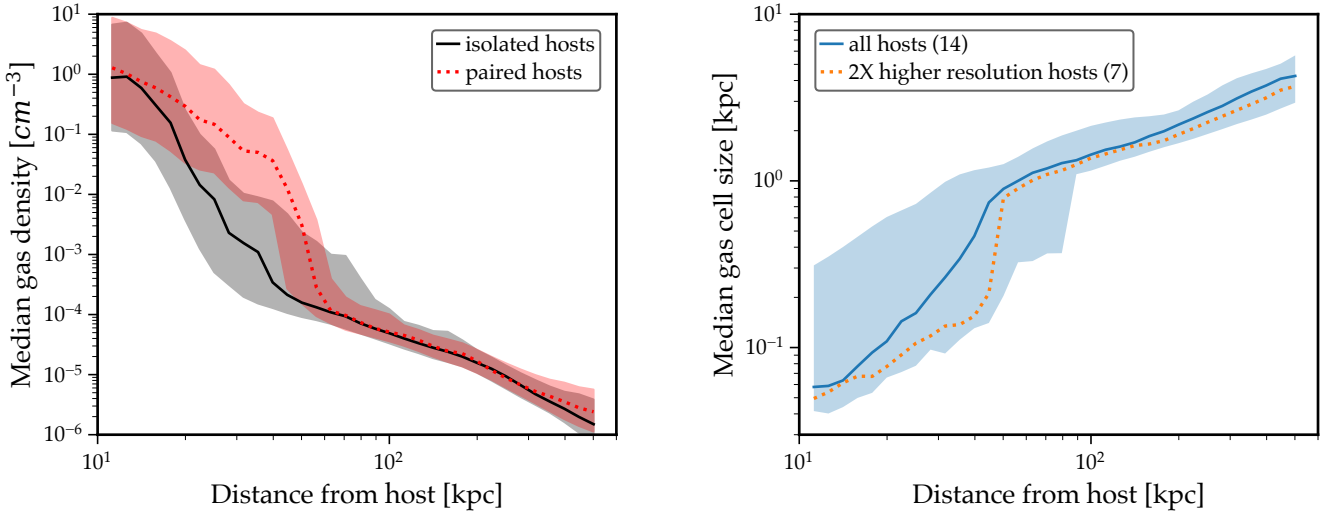


**Figure 2.** *Left:* The radial profile of CGM gas density around isolated and paired MW-mass hosts at  $z = 0$ . We show the median and 68 per cent variation in median density across the host populations. The median radial profiles of the isolated and paired hosts are nearly identical close to the disk ( $\lesssim 10$  kpc) and in the outer halo ( $\gtrsim 100$  kpc), but at  $20 - 50$  kpc the gas around paired hosts is up to two orders of magnitude more dense than the gas around isolated hosts. *Right:* The median resolution/gas cell size in the host CGM at  $z = 0$  ranges from  $\approx 0.06 - 4$  kpc within the host halos ( $10 - 500$  kpc from the host). Shaded regions are the 100 per cent host-to-host variations in their median gas cell sizes.

the disk well past the stellar disk ( $R \approx 15$  kpc) and into the halo ( $R \lesssim 50$  kpc). The stellar disks in the paired hosts are on average 15 – 25 per cent larger in radius than the isolated hosts, depending on the ages of the stellar populations (Garrison-Kimmel et al. 2018; Bellardini et al. 2022). As insets in the right panels of this figure, we show the disk of an isolated host (m12i) at the same scale. The gas disk of the isolated is clearly smaller in both radius and height. The size difference between isolated and paired hosts has the important consequence that satellites orbiting close to a paired host may feel higher ram pressure than satellites orbiting close to an isolated host. We explore this further in Section 3.5.

In Figure 2 (left), we show the radial profile of CGM gas density separately for isolated and paired hosts. We computed the volume-weighted median density in radial shells (35 log-spaced radial bins over  $10 - 500$  kpc) around each host i.e., we sorted the gas particles in each shell in increasing order of their size, and choose the density that corresponds to the median gas size (following Putman et al. 2021). We remove the satellite gas before calculating the CGM density to remove contamination from satellite ISM or recently stripped satellite gas. To exclude satellite gas from our measurements of the host halo, we identify the satellites present within the host halo using the halo catalogs and ignore any gas within  $10R_{*,1/2}$  and  $10\sigma$  of a satellite (similar to our method for gas assignment described in Section 2, but using a more liberal selection to omit recently stripped gas).

Figure 2 (left) shows that the host halo gas at  $z = 0$  is denser close to the hosts ( $\lesssim 60$  kpc). Going out from 20 to 60 kpc, the median density around paired hosts decreases by nearly three orders of magnitude for paired hosts compared to about one order of magnitude for isolated hosts. We explore this extended region of high density around the paired hosts further in Section 3.5. Beyond  $\sim 100$  kpc, the paired and isolated profiles are quite similar and have much smaller scatter. Though not shown here, we also note that for half of the hosts the median density in the inner CGM has also increased by about an order of magnitude over the last 10 Gyr.

Due to the Lagrangian nature of the hydrodynamic solver that we

use, the gas cell size (hydrodynamic smoothing kernel radius) scales with gas density such that regions of higher density are automatically better resolved. In Figure 2 (right), we show the average cell size in the host CGM versus distance from the host. Cell sizes range from  $\approx 100$  pc within the inner halo to  $\approx 4$  kpc in the outer halo. This trend in resolution shows that we do not resolve the clumpy CGM in the outer halo, and thus hydrodynamic interactions like ram pressure are likely under-resolved far from galaxies. However, given that we do not expect especially strong or effective ram pressure stripping far from galaxies, we focus our analysis on ram pressure close to the host/when galaxies are at small separations to mitigate hydrodynamic resolution effects.

### 3.2 Ram pressure histories

Figure 3 shows the median and 68 per cent variations in ram pressure versus time for different populations of low-mass galaxies in the simulations. We select all galaxies that are within 2 Mpc of a MW-mass host at  $z = 0$  and track their trajectories with merger trees. We calculate the ram pressure they experience as described in Section 2. We separate galaxies by their environment at each snapshot: satellites are within a MW-mass halo<sup>2</sup>, galaxies in low-mass groups are within the halo of a more massive dwarf galaxy, and centrals are not within a more massive halo. Low-mass group hosts typically have halo masses  $M_{200m} \approx 10^{9-11} M_\odot$  and stellar masses  $M_* \approx 10^{7-10} M_\odot$ . We note that individual galaxies may have belonged to all three groups at different times in the last 10 Gyr, but they are assigned to only a single group per snapshot.

As expected, MW satellites experience the highest levels of ram pressure throughout time, as they are in the most dense environment within the simulation volumes. Interestingly, ram pressure on

<sup>2</sup>  $d_{host}(t) < R_{200m,host}(t)$ , which yields 248 satellite galaxies at  $z = 0$  compared to 240 when using  $d_{host}(z = 0) < 300$  kpc because host radii are typically 300 – 400 kpc (Samuel et al. 2022).

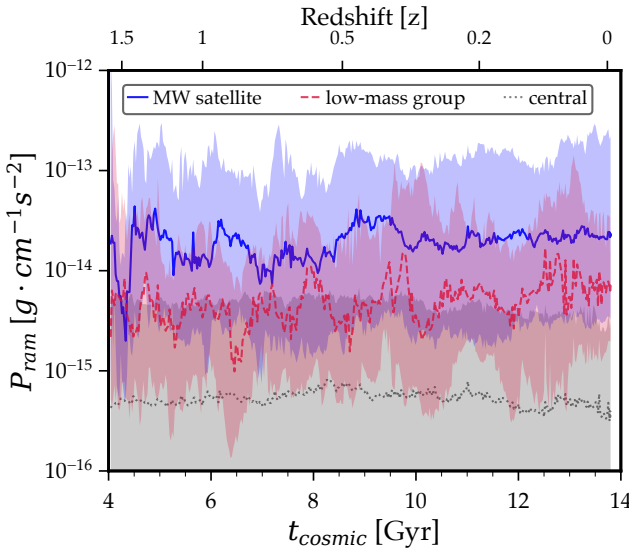


**Figure 3.** Ram pressure versus time for galaxies in different environments. Lines are medians and shaded regions are 68 per cent scatter across all galaxies and simulations. Ram pressure is highly variable over time and different environments experience characteristic/median levels of ram pressure. MW satellite galaxies typically experience the highest levels of ram pressure over time. However, galaxies in low-mass groups experience a level of ram pressure almost as high as that of MW satellites.

MW satellites is only about 4.6 times stronger on average than ram pressure on galaxies in low-mass groups. This difference is largely accounted for by different relative velocities between galaxies and ambient gas in the two environments: MW satellites have velocities that are about 2.2 times higher on average, which could account for up to a factor of 4.8 difference in ram pressure from the squared velocity component. Satellites have the highest velocity relative to ambient gas at  $\sim 100$  km/s, followed by galaxies in low-mass groups at  $\sim 40$  km/s, and centrals have the lowest at  $\sim 10$  km/s. However, the median ambient gas densities in low-mass groups are about 1.2 times those in MW halos, likely because galaxies in low-mass groups typically orbit within  $\lesssim 75$  kpc from the host, whereas most (surviving) MW satellite galaxies do not orbit within 50 kpc of the host. This may help explain why quenching is effective in low-mass group environments (Samuel et al. 2022). Centrals, on the other hand, experience relatively low levels of ram pressure likely due to the intergalactic medium and large scale filaments.

As evidenced by the noisy ram pressure histories, ram pressure is highly stochastic even within a given environment, but in a broad sense the median and scatter for each environment has stayed relatively flat over the last 10 Gyr. Interestingly, the ambient gas densities encountered by galaxies in low-mass groups or MW-mass halos have gradually increased over time and the relative velocities have decreased slightly for MW satellites.

Figure 4 shows a few examples of ram pressure histories for characteristic populations of low-mass galaxies. The two star-forming galaxies have relatively constant ram pressure that varies over about an order of magnitude in each case, however, the ram pressure on the star-forming MW satellite galaxy is about two orders of magnitude higher than the ram pressure on the star-forming central galaxy. In contrast, the ram pressure on the quiescent MW satellite galaxy varies over about six orders of magnitude, peaking near pericenter passages.

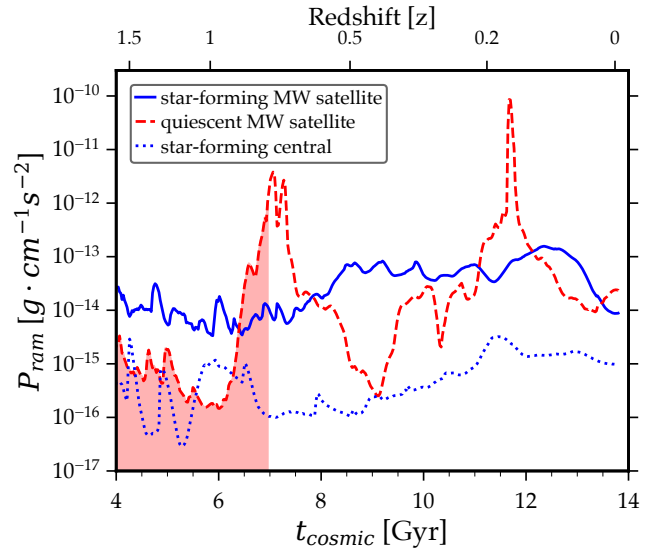


**Figure 4.** Examples of characteristic ram pressure histories for galaxies in different environments. The quiescent MW satellite has experienced significant spikes in ram pressure compared to the star-forming satellite and central galaxies. The shaded area under the curve indicates the integrated ram pressure felt by the quiescent MW satellite, measured from  $t = 4$  Gyr to when it quenches at  $t \approx 7$  Gyr.

### 3.3 Ram pressure required to quench

While observations of galaxies are limited to single snapshots in time of ram pressure effects, we are able to leverage ram pressure histories over the last 10 Gyr of the simulations with  $\approx 25$  Myr snapshot cadence. Here we explore the utility of various ram pressure summary statistics that take into account different aspects of the ram pressure histories that we measure: average, integrated, and maximum ram pressure.

We estimate ram pressure necessary to unbind gas and thus quench a galaxy ( $P_{ram, quench}$ ) using Equation 5, where  $\Sigma_{gas}(t)$  is the gas mass surface density within a galaxy over time and  $\Sigma_{dyn}(t)$  is the combined mass surface density of dark matter and stars within the halo over time (Gunn & Gott 1972). We calculate  $\Sigma_{gas}(t)$  as described in Section 2, and we follow a similar methodology for  $\Sigma_{dyn}(t)$  where we sum the stellar and dark matter masses of a galaxy/halo and divide by the cross-sectional area of the halo assuming spherical symmetry and using the halo radius ( $R_{200m}$ , defined using the dark matter distribution). We compute  $P_{ram, quench}$  at each snapshot within the last 10 Gyr, and take the maximum value over this time baseline, yielding an approximation of the maximal gravitational restoring force per unit area on the gas in a galaxy over time. We can therefore directly compare  $P_{ram, quench}$  to the ram pressure a galaxy experiences to get an idea of whether ram pressure is sufficient to strip gas from a galaxy.

$$P_{ram, quench} = \text{MAX}[2\pi \Sigma_{dyn}(t) \cdot \Sigma_{gas}(t)] \quad (5)$$

Figure 5 (left) shows the maximum ram pressure experienced by galaxies against our estimate of the ram pressure required to quench them. Note that we only include galaxies that contain gas and have not quenched before the 10 Gyr window where we measure ram pressure histories. Most of the galaxies above the one-to-one line are quiescent at  $z = 0$ , as expected because they have experienced higher ram pressure than necessary to quench. However, even though almost all of the star-forming galaxies lie below the line, as expected,

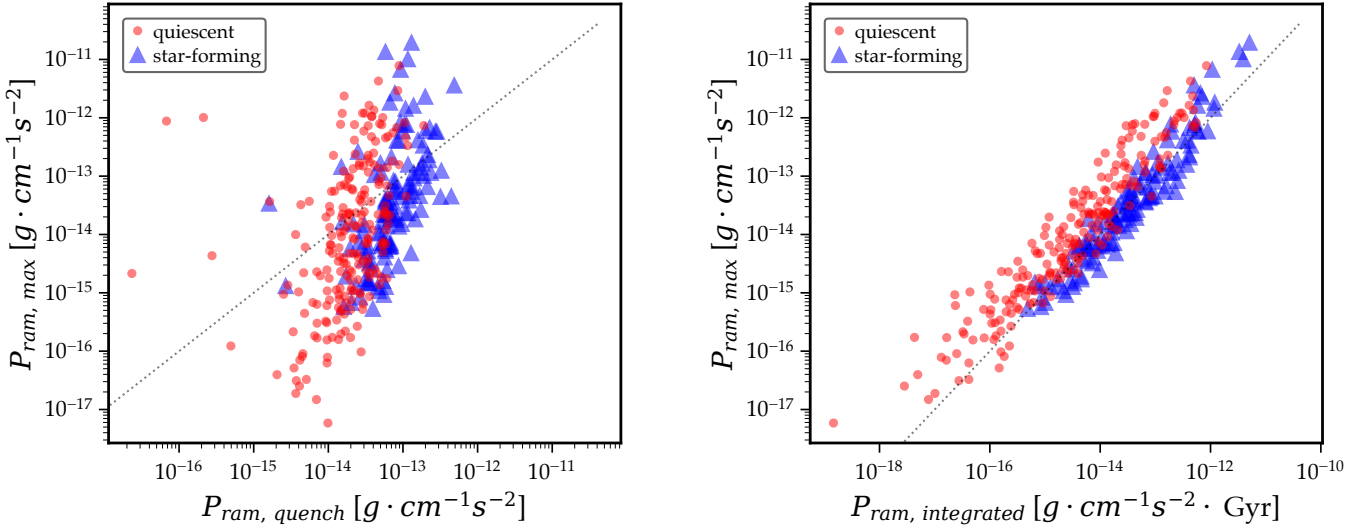


**Figure 5.** *Left:* Maximum ram pressure versus estimated ram pressure necessary to quench. Quiescent and star-forming galaxies follow a positive trend inclined relative to the one-to-one line, indicating that there is a more nuanced relationship between quenching and ram pressure than simply the maximal ram pressure experienced. Ram pressure alone may not have been sufficient to quench galaxies below the one-to-one line, and star-forming galaxies above it have managed to retain gas for star formation despite high levels of ram pressure. *Right:* Maximum ram pressure versus integrated ram pressure. Quiescent and star-forming galaxies separate more cleanly in this space. In particular, quiescent galaxies typically lie above the one-to-one line and star-forming galaxies lie along it. This indicates that quiescent galaxies feel a strong spike in ram pressure, with a characteristic average ratio of the peak to integrated values.

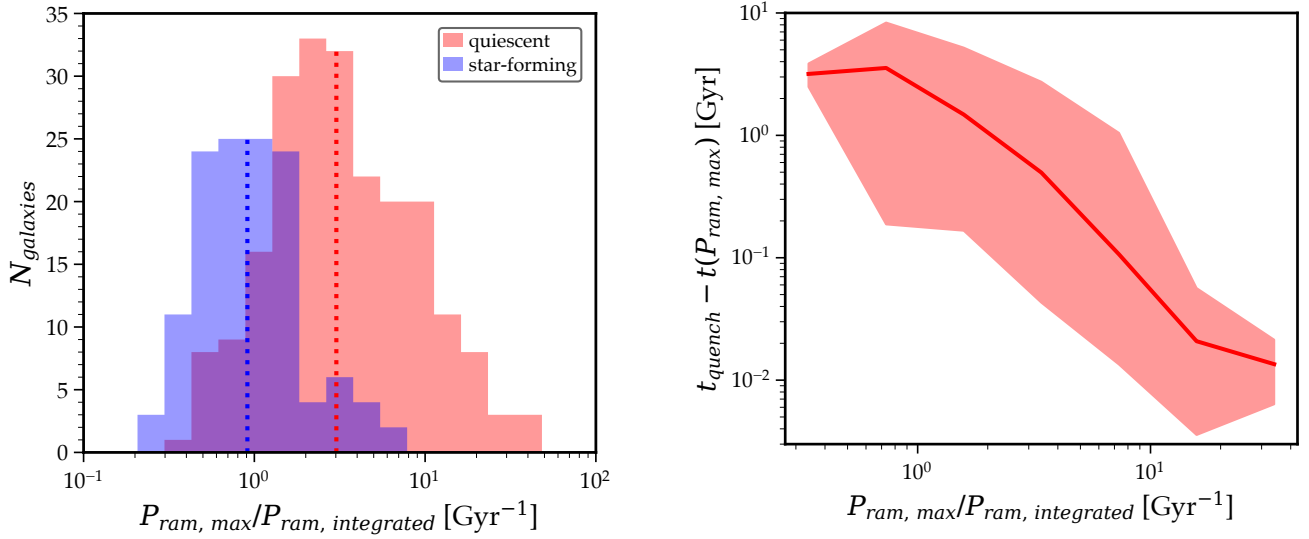


**Figure 6.** *Left:* Histogram of the ram pressure impulsiveness for galaxies in our sample. Lines mark the median values of each distribution. Galaxies with an impulsiveness above 2 are highly likely to be quiescent. *Right:* The timescale/quenching delay time between maximum ram pressure and quenching as a function of the impulsiveness of ram pressure. The typical quenching delay time substantially decreases (from 3 Gyr to  $\approx 20$  Myr) as impulsiveness increases from 0.2 to 40. Once impulsiveness reaches  $\gtrsim 2$ , galaxies quench in under 1 Gyr on average, marking the transition from smooth to bursty ram pressure stripping.

there is also a significant population of quiescent galaxies below the line. The quiescent galaxies below the line may indicate the effectiveness of other processes like stellar feedback in quenching galaxies. The scatter of both quiescent and star-forming galaxies above and below the one-to-one line and the fact that their trends are inclined relative to this line, show that maximum ram pressure and our simple estimate of ram pressure required to quench cannot fully disentangle the quiescent and star-forming populations.

We can also leverage the long time baseline of ram pressure histories in our simulations to explore how much ram pressure quiescent galaxies have experienced in total. Figure 4 demonstrates one of the defining features of the ram pressure histories of quiescent galaxies: large peaks above a relatively flat baseline. We use this fact to motivate a measure of the maximum ram pressure strength against the baseline ram pressure. The impulsiveness/burstiness ( $R_{\text{max/int}}$ ) of ram pressure is defined in Equation 6 (in units of  $\text{Gyr}^{-1}$ ) as the ratio

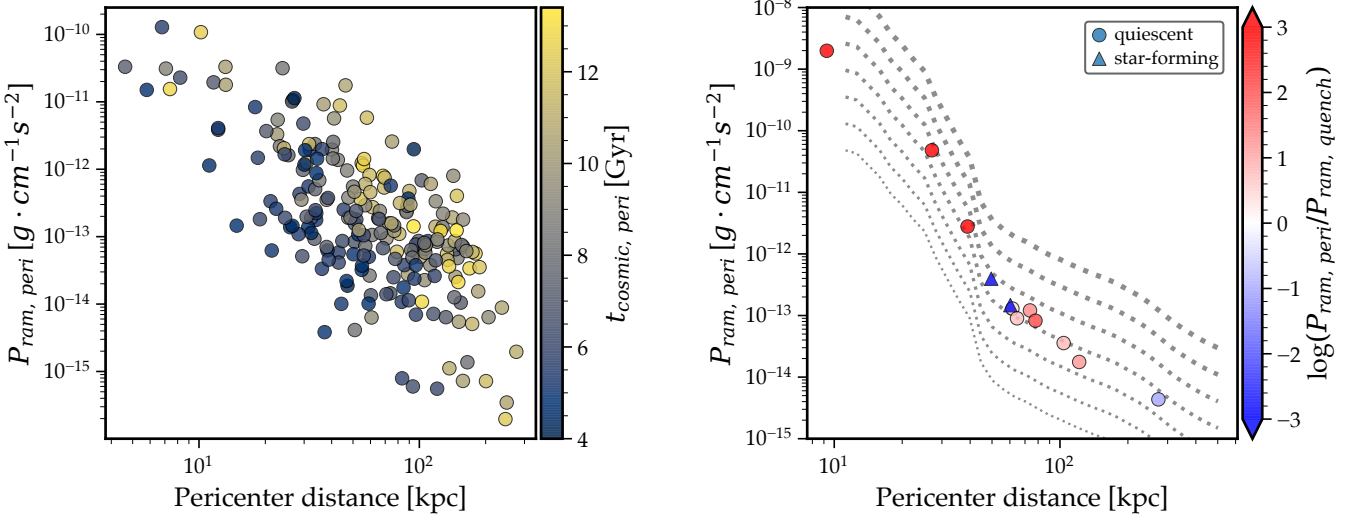


**Figure 7.** *Left:* Ram pressure on satellite galaxies that are quiescent at  $z = 0$  during the pericenter passages that occurred closest to their quenching times. Ram pressure during pericenter passage rises sharply with decreasing distance to the host. At fixed distance, more recent pericenter passages are typically associated with higher ram pressure because the median CGM density in the inner host halo increases near  $z = 0$ . *Right:* Estimated ram pressure on observed MW satellite galaxies at their most recent pericenter passage. Lines are ram pressure profiles at fixed velocities (50 – 1000 km/s). Points are colored by the ratio of ram pressure at pericenter to ram pressure required to quench. The estimates using the simulations are similar to observations of MW satellites: most galaxies, except the Magellanic Clouds (blue triangles), are likely to be quiescent at  $z = 0$  based upon having experienced greater or similar ram pressure compared to their current  $P_{\text{ram}, \text{quench}}$ .

of maximum ram pressure to total integrated ram pressure *prior to quenching*, where the sum for integrated ram pressure is done over snapshots and the average inter-snapshot spacing is  $\Delta t \approx 25$  Myr. The integrated ram pressure,  $P_{\text{ram}, \text{integrated}}$ , is similar to what Simons et al. (2020) call the surface momentum density.

In general, integrated ram pressure increases with galaxy stellar mass, from  $\sim 10^{-17}$  to  $\sim 10^{-12} \text{ g} \cdot \text{cm}^{-1} \text{s}^{-2}$ /Gyr because it takes higher and more prolonged ram pressure to quench more massive galaxies. Integrated ram pressure is depicted in Figure 4 as the red shaded region underneath the ram pressure history of the quiescent MW satellite. We can see that just before quenching, the galaxy experiences a surge in ram pressure of over three orders of magnitude. Using Equation 6, we find that the quiescent satellite galaxy has  $R_{\text{max/int}} \approx 11 \text{ Gyr}^{-1}$ , compared to  $R_{\text{max/int}} \approx 0.4 \text{ Gyr}^{-1}$  for the ram pressure histories of the two star-forming galaxies shown.

$$R_{\text{max/int}} = \frac{P_{\text{ram}, \text{max}}}{P_{\text{ram}, \text{integrated}}} = \frac{\text{MAX}(P_{\text{ram}}(t))}{\sum_i (P_{\text{ram}}(t) \cdot \Delta t)} \quad (6)$$

Figure 5 (right) shows the maximum ram pressure experienced by galaxies against their integrated ram pressure. The populations of quiescent and star-forming galaxies separate along two parallel but offset relations in this space, with some overlapping scatter. Star-forming galaxies are concentrated along the one-to-one line, while quiescent galaxies almost always lie above this line. We quantify this dichotomy further in Figure 6 (left), which shows a histogram of the ratio of these two quantities,  $R_{\text{max/int}}$ . The distribution for star-forming galaxies peaks around unity while the quiescent distribution peaks around  $R_{\text{max/int}} \approx 2–3$ . The star-forming distribution has a small tail to higher  $R_{\text{max/int}}$ , but in general galaxies with  $R_{\text{max/int}} \gtrsim 2$  are highly likely to be quiescent.

In Figure 6 (right), we show the delay time between quenching and maximum ram pressure ( $t_{\text{quench}} - t(P_{\text{ram}, \text{max}})$ , which is positive by definition) versus the impulsiveness of maximum ram pressure.

Quenching delay time relative to maximum ram pressure is highly correlated with the impulsiveness of ram pressure. In particular, once ram pressure exceeds an impulsiveness/burstiness of  $R_{\text{max/int}} \gtrsim 2$ , the quenching delay time typically drops below 1 Gyr. Interestingly, for impulsiveness values  $\gtrsim 10$ , quenching delay times drop to at or below a few tens of Myr, indicating rapid quenching via ram pressure stripping when a galaxy experiences a strong burst of ram pressure relative to its integrated ram pressure. We recover similar trends when comparing this quenching delay time to  $P_{\text{ram}, \text{max}} / P_{\text{ram}, \text{quench}}$ , but the correlation is stronger with impulsiveness.

### 3.4 Ram pressure at pericenter

Because the CGM in the inner host halo is denser than in the outer host halo (see Section 3.1), and because satellites move fastest in their orbits when they are near pericenter, we expect that satellites should feel stronger ram pressure during pericenter passages. Figure 7 shows the effects of inner CGM density enhancement on the ram pressure that satellite galaxies experience during the pericenter passage that occurs closest to when they quench. Ram pressure at pericenter ( $P_{\text{ram}, \text{peri}}$ ) increases by about four orders of magnitude as pericenter distance decreases from  $\approx 100$  kpc to  $\approx 10$  kpc. The order of magnitude increase in inner CGM density of some hosts at late times also drives a secondary trend in ram pressure at pericenter passage whereby ram pressure is higher for more recent pericenter passages at a fixed distance.

Even though the median host CGM densities that we presented in Figure 2 (left) do not accurately represent the clumpy nature of the host CGM, we can still use them to estimate the average ram pressure felt by observed MW satellite galaxies, and weigh this against the ram pressure required to quench them. Figure 7 (right) shows the estimated ram pressure on 12 MW satellites at pericenter at their pericenter distance. To obtain the points on this figure, we integrated the orbits of MW satellites over 10 Gyr using galpy and the host

galaxy/halo potential MWPotential2014. We saved the distance and velocity at pericenter, and mapped the distance to a host CGM density using the median radial density profile across all of the hosts. The curves in the background show ram pressure throughout the halo at fixed velocities (50–1000 km/s, in log-spaced bins). The shape of the points indicates whether they are quiescent ( $M_{\text{HI}}/M_{\text{dyn}} \leq 0.1$ ) or star-forming ( $M_{\text{HI}}/M_{\text{dyn}} > 0.1$ ). We take values of  $M_{\text{HI}}$  and  $M_{\text{dyn}}$  from Putman et al. (2021) and McConnachie (2012), respectively.

By scaling the ram pressure at pericenter to the ram pressure required to quench a galaxy, we can see that the star-forming galaxies (the Magellanic Clouds, represented by blue triangles) have not experienced enough ram pressure to quench, while the remaining galaxies are quiescent and have ratios of  $P_{\text{ram}, \text{peri}}/P_{\text{ram}, \text{quench}}$  above unity. The one exception is the quiescent MW satellite galaxy Leo I with a pericenter distance near the edge of the host halo that has not brought it into a dense enough region for ram pressure at pericenter to surpass  $P_{\text{ram}, \text{quench}}$ . However, we stress that it may have encountered a dense clump of gas in the host halo or elsewhere that our simple estimate using median host CGM density cannot account for.

If we instead were to color the points by the impulsiveness of ram pressure experienced at pericenter, where we measured integrated ram pressure from 10 Gyr ago until when they formed 90 per cent of their stars (Weisz et al. 2015), then almost every galaxy has experienced enough ram pressure to quench ( $P_{\text{ram}, \text{peri}}/P_{\text{ram}, \text{integrated}} > 1$ ) except the Sagittarius dSph, SMC, Fornax, and Leo II (although Leo II’s ratio is close to unity at 0.73). Draco and Leo I quench before coming within 500 kpc of a host and are thus excluded from this exercise. This shows that even neglecting the clumpy nature of the CGM, ram pressure can account for quenching many of the observed MW satellite galaxies. It also implies that the LMC may be quenched shortly after pericenter passage, and combined with the fact that it is currently star-forming agrees with the idea that it is at its first pericenter passage (e.g., Kallivayalil et al. 2013).

### 3.5 Angular anisotropy in inner host CGM

In light of recent work finding anisotropic quenching in massive galaxy clusters (e.g., Martín-Navarro et al. 2021), we search for similar signals close to the host disks in our simulations. We quantify density, ram pressure, and quenching with respect to galactocentric latitude ( $\beta$ ), or angle off of the host disk, as defined by a Cartesian coordinate system centered on the host halo with  $z$  axis perpendicular to the host disk and  $x$  and  $y$  axes aligned with the host disk. Note that we measure  $\beta$  from the host halo center, in contrast to the standard galactic latitude ( $b$ ) that is measured from the solar position. See Equation 3.5 for the mathematical expression of latitude and Figure 8 (left) for visual depiction of latitude. We use only the absolute value of  $\beta$  such that we treat measurements above and below the host disk equally, because we do not have a sufficient number of systems in order to leverage positive versus negative latitudes.

$$\beta = \arctan \left( \frac{z^2}{\sqrt{x^2 + y^2}} \right) \quad (7)$$

Figure 8 shows the ratio of density in low latitude regions ( $0^\circ \leq |\theta| < 30^\circ$ ) to density in higher latitude regions ( $30^\circ \leq |\theta| < 90^\circ$ ) at  $z = 0$ . The ratio is relatively flat and near unity at 80–400 kpc, which indicates that the density in the low and high latitude regions are roughly equal in the outer host halo. However, within

$\lesssim 100$  kpc the ratio increases by 1 and 2.5 orders of magnitude for isolated and paired hosts, respectively. We checked if this feature was gas temperature-dependent by using temperature cuts of  $10^4$  K, and found that quite a lot of the 3 kpc shells do not have any gas below that temperature.

Figure 9 (left) shows the ram pressure experienced by satellite galaxies that orbit within 50 kpc of a MW-mass host over the last 5 Gyr, as a function of galactocentric latitude. The lines shows the medians and the shaded regions shows the 68 per cent scatter of all snapshots of satellite orbits meeting these criteria. The ram pressure experienced by simulated satellite galaxies scatters to higher values at small angles around the paired hosts compared to the isolated hosts. The median ram pressure for satellites of paired hosts tends to be equal to or greater than that for satellites of isolated hosts at all latitudes.

Figure 9 (right) shows the quiescent fraction of satellite galaxies versus their angle off of the host galaxy disk. The quiescent fraction for simulated paired hosts shows a distinct rise as latitude decreases, whereas the quiescent fraction for isolated hosts rises only gradually. The quiescent fraction of observed LG galaxies has a slight rise at angles  $\lesssim 60^\circ$ , but the population is fully quiescent at  $\gtrsim 60^\circ$ . If we restrict the satellite stellar mass to  $M_* > 10^6 M_\odot$ , we obtain essentially the same results for the observations and the simulated satellites around paired hosts, however, we also recover a similar trend of increased quiescent fraction at low latitudes for the simulated satellites around isolated hosts. We note that the trends with this angular coordinate are marginal for the LG because of small numbers of observed satellites per angular bin. We interpret the simulation trends in quiescent fraction with angle as being due to increased ram pressure from the higher density CGM at low angles from the host disk.

Our results are qualitatively similar to a few recent studies that have found signals of anisotropic quenching within both simulated and observed massive galaxy clusters. Martín-Navarro et al. (2021) first reported a statistically significant enhancement of the quiescent fraction of galaxies near the major axis of the brightest cluster galaxies in SDSS ( $M_{\text{halo}} \sim 10^{12-14} M_\odot$  and median  $z = 0.08$ ). Based on their analysis of a similar signal in the TNG simulations, they concluded that AGN feedback drives anisotropy in the host CGM density which in turn drives anisotropy in ram pressure and quenching. Since this study, others have found anisotropic quenching in massive clusters with SDSS (Zhang & Zaritsky 2022) and at higher redshift ( $z \lesssim 1.25$ ) using CLASH and HSC-SSP (Stott 2022; Ando et al. 2022).

Interestingly, Stott (2022) proposed an alternative explanation for anisotropic ram pressure and quenching that does not rely on AGN feedback. Stott (2022) suggests that elongation of the CGM and intracluster medium out to large distances around a BCG, similar to the ellipsoidal shape of the BCG itself, could also produce higher ram pressure at low angles from the BCG major axis. Given the lack of AGN feedback in our simulations, the alternative explanation put forth by Stott (2022) seems sufficient to explain both the enhanced CGM density, quiescent fraction, and ram pressure at low angles from host disks that we find here.

## 4 CONCLUSIONS

We have examined the ram pressure experienced by low-mass galaxies in simulations of Local Group-like environments. We have found several trends relating ram pressure and quenching to different aspects of a low-mass galaxy’s evolution such as its environment, max-

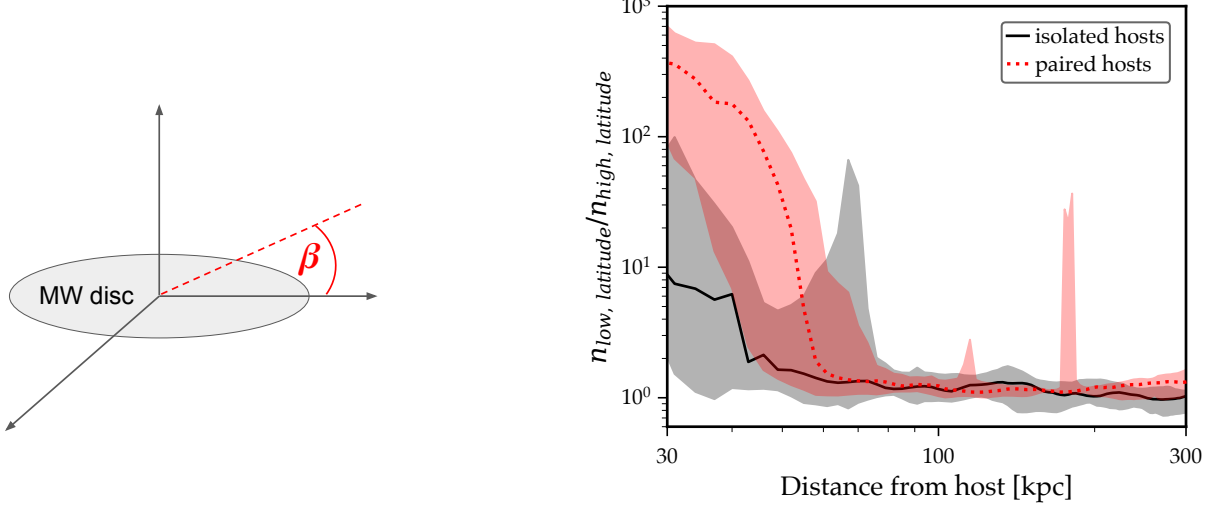


**Figure 8.** *Left:* Schematic of how we measured galactocentric latitude ( $\beta$ ) as the angle off of the host galaxy disk. *Right:* The ratio of median CGM number density in low latitudes ( $|\beta| \leq 30^\circ$ ) to density in higher latitude regions ( $30^\circ < |\beta| \leq 90^\circ$ ) at  $z = 0$  as a function of distance from the host. The shaded regions are the 68 per cent host-to-host variations. The large spikes near 100 and 200 kpc for the paired host distribution are from the gas overdensities visible near the host disk plane of Louise in the right panels of Figure 1.

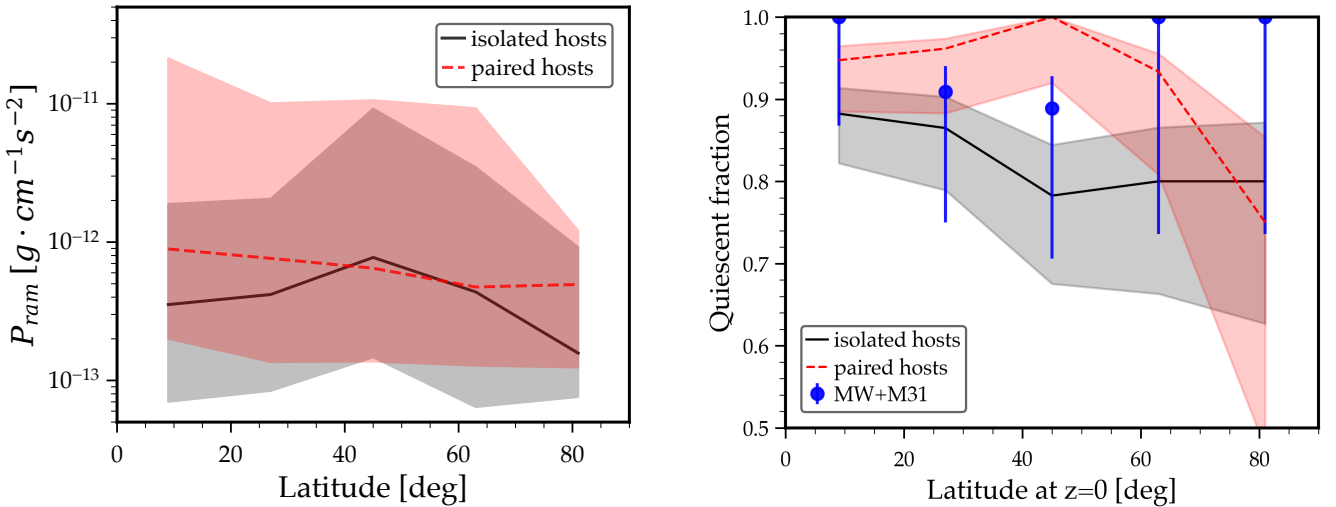


**Figure 9.** *Left:* Ram pressure experienced by surviving satellite galaxies that have orbited within 50 kpc of a host as a function of latitude. Lines are medians and shaded regions are 68 per cent variations across hosts, satellites, and time. Satellites of paired hosts experience slightly higher ram pressure at lower latitudes compared to satellites of isolated hosts. *Right:* The quiescent fraction of  $z = 0$  satellites as a function of their latitude or angular position off of the host galaxy disk. The quiescent fraction of observed LG satellites sharply and monotonically rises from 60 to 0 degrees, and is noisier from 60 to 90 degrees. Satellites around paired (LG-like) hosts in the simulations have a noticeable increase in quiescent fraction as latitude decreases from 75 to 30 degrees, whereas the quiescent fraction of satellites around isolated hosts rises only slightly from 90 to 0 degrees. Satellites around MW-mass paired hosts are marginally preferentially quenched closer to the host galaxy disk.

imum and integrated ram pressure prior to quenching, pericenter passage, and presence in the halo of a paired (Local Group-like) versus isolated MW-mass host. Below, we list each of our conclusions.

(i) Ram pressure on MW satellite galaxies is only 4.6 times higher on average than ram pressure on galaxies in low-mass groups. This helps explain why group-preprocessing is an effective quenching mechanism for low-mass LG satellites.

(ii) Quiescent galaxies have experienced burstier ram pressure on average. We quantify the burstiness of ram pressure ( $R_{\text{max/int}}$ ) by

scaling the maximum ram pressure to the integrated ram pressure. We find that galaxies with  $R_{\text{max/int}} \gtrsim 2$  are highly likely to be quiescent, whereas galaxies with  $R_{\text{max/int}} \lesssim 1$  are typically star-forming. Thus, ram pressure may need to be significantly bursty to quench a galaxy.

(iii) The time between maximum ram pressure and quenching strongly correlates with the burstiness of ram pressure ( $R_{\text{max/int}}$ ). At  $R_{\text{max/int}} \gtrsim 2$ , the quenching delay time lowers below 1 Gyr and decreases to tens of Myr at  $R_{\text{max/int}} \gtrsim 10$ . Therefore, the burstiness of ram pressure may also dictate how rapidly quenching proceeds.

(iv) Ram pressure rises sharply with decreasing distance to the host. Ram pressure increases by about four orders of magnitude going from 100 to 10 kpc from the host. At fixed distance, more recent pericenter passages are also typically associated with 1 – 2 orders of magnitude higher ram pressure.

(v) The host CGM density is larger in the inner halo compared to the outer halo by 2 – 4 orders of magnitude on average across our sample of 14 hosts. The density at a fixed radius at in the inner halo can vary by up to 2 orders of magnitude across the different hosts.

(vi) The CGM density around paired hosts varies as a function of angle off of the host disk, or latitude, whereby density is enhanced by  $\approx 2$  orders of magnitude at small angles ( $< 30^\circ$ ) and small distances ( $\lesssim 100$  kpc) from the disk compared to larger angles. The CGM around isolated hosts shows a less significant and noisier density enhancement of  $\lesssim 1$  order of magnitude at low latitudes. The ram pressure histories of close-orbiting ( $< 50$  kpc) satellites around paired hosts scatter to higher values than satellites of isolated hosts.

(vii) The density and ram pressure enhancements at low latitudes is also reflected in a larger quiescent fraction of ( $z = 0$ ) satellite galaxies at  $\lesssim 60^\circ$  around the paired hosts compared to the isolated hosts. These results are reminiscent of recent results showing a more statistically significant signal of anisotropic quenching around massive galaxy clusters.

#### 4.1 Discussion

Our analysis shows that quiescent galaxies are more likely to have experienced highly impulsive/peaked ram pressure just before quenching. In contrast, even MW satellite galaxies may remain star-forming for long periods of time if their ram pressure histories are relatively constant or smooth. Smooth ram pressure likely does not quenching galaxies on short timescales but rather acts over a prolonged timescale and contributes to a starvation mode of quenching, whereas bursty/impulsive ram pressure effectively strips the ISM on timescales as short as a few tens of Myr. Our results are in broad agreement with the idea of smooth ram pressure stripping removing gas from the outskirts/CGM of a galaxy, but not the ISM. For example, McCarthy et al. 2008 used hydrodynamic simulations to test an analytical model for ram pressure stripping, and found that gas loss ceases when ram pressure and restoring force are roughly equal, which leads to incomplete gas removal even after 10 Gyr. Furthermore, our results support the findings of work from idealized simulations that showed that comparisons between simulations and observations must take the variation of the ram pressure profile due to a galaxy’s orbit into consideration, as the most profound quenching effects are felt near pericenter (Tonnesen 2019).

It is interesting to compare our results on ram pressure with those from Simons et al. 2020, who examined the ram pressure histories around six MW-mass hosts from the FOGGIE simulations with high resolution in the host CGM. Lagrangian hydrodynamic simulations (like the FIRE simulations we use here) have higher resolution in higher density regions like a galactic disc, which leaves the lower-density CGM comparatively under-resolved. However, FOGGIE purposefully simulates the CGM around MW-mass galaxies at high spatial resolution using the grid-based code Enzo and a forced refinement scheme that pre-tracks the halo of interest in a lower resolution run. The MW-mass host halos of the FOGGIE simulations are uniformly resolved with cell sizes of  $\approx 100 – 200$  pc, and the resolution sharply degrades to  $\approx 3 – 5$  kpc beyond  $2R_{vir} \sim 700$  kpc (Peeples et al. 2019). Comparatively, our simulations achieve similar resolution in the host halos on average: in the innermost regions ( $< 20$  kpc) the resolution actually surpasses FOGGIE as cell sizes

can reach values down to  $\approx 60$  pc, around 30-40 kpc our cell sizes are roughly equal to FOGGIE’s (200 pc), and our cell size gradually increases to about 4 kpc at 500 kpc from the hosts.

Though Simons et al. 2020 concentrate their analysis on  $z \geq 2$  (prior when we measure ram pressure histories) because not all simulations were run to  $z = 0$ , our results are still qualitatively similar, as they find high stochasticity in ram pressure on individual galaxies and throughout the host halos.

A caveat to our work is that we only examine the ram pressure histories of galaxies that survive to  $z = 0$ . We may be missing galaxies that experience impulsive ram pressure stripping but are also gravitationally disrupted and/or not identified by the halo finder. In particular, in our analysis of anisotropy in the host CGM (Section 3.5), we have examined the ram pressure histories of surviving, close-orbiting satellites ( $d_{host} < 50$  kpc). If we included galaxies that disrupted before  $z = 0$  in our analysis, we could increase the number of ram pressure histories that we examine, but with little connection to observed satellite galaxies at  $z = 0$ . However, this exclusion is unlikely to change our results on star-forming galaxies, which are less likely to be disrupted.

We have also not explicitly examined the role of stellar feedback as an alternative or complementary mechanism to ram pressure in quenching low-mass galaxies. In particular, supernovae can rarefy and eject a galaxy’s interstellar medium (ISM), which may then cause it to be more easily removed by ram pressure (El-Badry et al. 2016). Rey et al. (2022) found that the spatial extent of gas in simulated low-mass galaxies varied significantly over timescales of a few Gyr due to stellar feedback. While this extended gas may be re-accreted onto isolated galaxies, an ejection event occurs within a dense host halo environment, the gas may be more easily removed by ram pressure.

Moreover, we have not yet explored the detailed and well-studied role of ram pressure *inducing* star formation in galaxies (e.g., Tonnesen & Bryan 2009; Genina et al. 2019; Wright et al. 2019; Hausammann et al. 2019; Di Cintio et al. 2021). Most of these studies have focused on satellites of massive hosts like the MW, but the connection between ram pressure in low-mass groups and induced star formation remains to be explored. In particular, Massana et al. 2022 recently showed that star formation in the LMC and SMC was correlated over the last  $\sim 3.5$  Gyr. In future work we will look for such correlations in simulated low-mass groups outside of a MW halo or between satellite-satellite pairs within a MW halo.

#### ACKNOWLEDGEMENTS

JS was supported by an NSF Astronomy and Astrophysics Postdoctoral Fellowship under award AST-2102729. BP received support from the REU program at UC Davis through NSF grant PHY-1852581. JS and AW received support from: NSF grants CAREER 2045928 and 2107772; NASA ATP grants 80NSSC18K1097 and 80NSSC20K0513; HST grants AR-15057, AR-15809, GO-15902 from the Space Telescope Science Institute (STScI), which is operated by the Association of Universities for Research in Astronomy, Inc., for NASA, under contract NAS5-26555; a Scialog Award from the Heising-Simons Foundation; and a Hellman Fellowship.

We performed this work in part at the Aspen Center for Physics, supported by NSF grant PHY-1607611, and at the KITP, supported by NSF grant PHY-1748958.

We ran simulations using the Extreme Science and Engineering Discovery Environment (XSEDE), supported by NSF grant ACI-1548562; Frontera allocations AST21010 and AST20016, supported by the NSF and TACC; Blue Waters via allocation PRAC

NSF.1713353 supported by the NSF; the NASA HEC Program through the NAS Division at Ames Research Center.

We gratefully acknowledge use of the IPython package (Pérez & Granger 2007), NumPy (Harris et al. 2020), SciPy (Jones et al. 2001), Numba (Lam et al. 2015), matplotlib (Hunter 2007), and galpy (Bovy 2015).

## DATA AVAILABILITY

The FIRE-2 simulations are publicly available (Wetzel et al. 2022) at <http://flatHub.flatironinstitute.org/fire>. Additional FIRE simulation data is available at <https://fire.northwestern.edu/data>. A public version of the GIZMO code is available at <http://www.tapir.caltech.edu/~phopkins/Site/GIZMO.html>. The publicly available software packages used to analyze these data are available at: [https://bitbucket.org/awetzel/gizmo\\_analysis](https://bitbucket.org/awetzel/gizmo_analysis), [https://bitbucket.org/awetzel/halo\\_analysis](https://bitbucket.org/awetzel/halo_analysis), and <https://bitbucket.org/awetzel/utilities> (Wetzel & Garrison-Kimmel 2020b,a).

## REFERENCES

- Ando M., Shimasaku K., Ito K., 2022, arXiv e-prints, p. arXiv:2209.00015
- Bellardini M. A., Wetzel A., Loebman S. R., Bailin J., 2022, *MNRAS*, **514**, 4270
- Bovy J., 2015, *ApJS*, **216**, 29
- Di Cintio A., Mostoghiu R., Knebe A., Navarro J. F., 2021, *MNRAS*, **506**, 531
- El-Badry K., Wetzel A., Geha M., Hopkins P. F., Kereš D., Chan T. K., Faucher-Giguère C.-A., 2016, *ApJ*, **820**, 131
- Escala I., et al., 2018, *MNRAS*, **474**, 2194
- Faucher-Giguère C.-A., Lidz A., Zaldarriaga M., Hernquist L., 2009, *ApJ*, **703**, 1416
- Fillingham S. P., Cooper M. C., Wheeler C., Garrison-Kimmel S., Boylan-Kolchin M., Bullock J. S., 2015, *MNRAS*, **454**, 2039
- Garrison-Kimmel S., et al., 2018, *MNRAS*, **481**, 4133
- Garrison-Kimmel S., et al., 2019a, *MNRAS*, **487**, 1380
- Garrison-Kimmel S., et al., 2019b, *MNRAS*, **489**, 4574
- Genina A., Frenk C. S., Benítez-Llambay A., Cole S., Navarro J. F., Oman K. A., Fattahi A., 2019, *MNRAS*, **488**, 2312
- Grcevich J., Putman M. E., 2009, *ApJ*, **696**, 385
- Gunn J. E., Gott J. Richard I., 1972, *ApJ*, **176**, 1
- Hafen Z., et al., 2019, *MNRAS*, **488**, 1248
- Hahn O., Abel T., 2011, *MNRAS*, **415**, 2101
- Harris C. R., et al., 2020, *Nature*, **585**, 357
- Hausammann L., Revaz Y., Jablonka P., 2019, *A&A*, **624**, A11
- Hopkins P. F., 2015, *MNRAS*, **450**, 53
- Hopkins P. F., 2016, *MNRAS*, **455**, 89
- Hopkins P. F., et al., 2018a, *MNRAS*, **477**, 1578
- Hopkins P. F., et al., 2018b, *MNRAS*, **480**, 800
- Hunter J. D., 2007, *Computing In Science & Engineering*, **9**, 90
- Jones E., Oliphant T., Peterson P., et al., 2001, SciPy: Open source scientific tools for Python, <http://www.scipy.org/>
- Kallivayalil N., van der Marel R. P., Besla G., Anderson J., Alcock C., 2013, *ApJ*, **764**, 161
- Krumholz M. R., Gnedin N. Y., 2011, *ApJ*, **729**, 36
- Lam S. K., Pitrou A., Seibert S., 2015, in Proceedings of the Second Workshop on the LLVM Compiler Infrastructure in HPC. LLVM '15. ACM, New York, NY, USA, pp 7:1–7:6, doi:10.1145/2833157.2833162, <http://doi.acm.org/10.1145/2833157.2833162>
- Martín-Navarro I., Pillepich A., Nelson D., Rodriguez-Gomez V., Donnari M., Hernquist L., Springel V., 2021, *Nature*, **594**, 187
- Massana P., et al., 2022, arXiv e-prints, p. arXiv:2203.09523
- McCarthy I. G., Frenk C. S., Font A. S., Lacey C. G., Bower R. G., Mitchell N. L., Balogh M. L., Theuns T., 2008, *MNRAS*, **383**, 593
- McConnachie A. W., 2012, *AJ*, **144**, 4
- Pasha I., Mandelker N., van den Bosch F. C., Springel V., van de Voort F., 2022, arXiv e-prints, p. arXiv:2204.04097
- Peeples M. S., et al., 2019, *ApJ*, **873**, 129
- Pérez F., Granger B. E., 2007, *Computing in Science and Engineering*, **9**, 21
- Planck Collaboration et al., 2018, arXiv e-prints, p. arXiv:1807.06209
- Putman M. E., Zheng Y., Price-Whelan A. M., Grcevich J., Johnson A. C., Tollerud E., Peek J. E. G., 2021, *ApJ*, **913**, 53
- Rey M. P., Pontzen A., Agertz O., Orkney M. D. A., Read J. I., Saintonge A., Kim S. Y., Das P., 2022, *MNRAS*,
- Samuel J., et al., 2020, *MNRAS*, **491**, 1471
- Samuel J., Wetzel A., Chapman S., Tollerud E., Hopkins P. F., Boylan-Kolchin M., Bailin J., Faucher-Giguère C.-A., 2021, *MNRAS*, **504**, 1379
- Samuel J., Wetzel A., Santistevan I., Tollerud E., Moreno J., Boylan-Kolchin M., Bailin J., Pardasani B., 2022, *MNRAS*, **514**, 5276
- Santistevan I. B., Wetzel A., El-Badry K., Bland-Hawthorn J., Boylan-Kolchin M., Bailin J., Faucher-Giguère C.-A., Benincasa S., 2020, *MNRAS*, **497**, 747
- Simons R. C., et al., 2020, *ApJ*, **905**, 167
- Springel V., 2005, *MNRAS*, **364**, 1105
- Stott J. P., 2022, *MNRAS*, **511**, 2659
- Su K.-Y., Hopkins P. F., Hayward C. C., Faucher-Giguère C.-A., Kereš D., Ma X., Robles V. H., 2017, *MNRAS*, **471**, 144
- Tonnesen S., 2019, *ApJ*, **874**, 161
- Tonnesen S., Bryan G. L., 2009, *ApJ*, **694**, 789
- Weisz D. R., Dolphin A. E., Skillman E. D., Holtzman J., Gilbert K. M., Dalcanton J. J., Williams B. F., 2015, *ApJ*, **804**, 136
- Wetzel A., Garrison-Kimmel S., 2020a, HaloAnalysis: Read and analyze halo catalogs and merger trees (ascl:2002.014)
- Wetzel A., Garrison-Kimmel S., 2020b, GizmoAnalysis: Read and analyze Gizmo simulations (ascl:2002.015)
- Wetzel A. R., Deason A. J., Garrison-Kimmel S., 2015, *ApJ*, **807**, 49
- Wetzel A. R., Hopkins P. F., Kim J.-h., Faucher-Giguère C.-A., Kereš D., Quataert E., 2016, *ApJ*, **827**, L23
- Wetzel A., et al., 2022, arXiv e-prints, p. arXiv:2202.06969
- Wright A. C., Brooks A. M., Weisz D. R., Christensen C. R., 2019, *MNRAS*, **482**, 1176
- Yang Y., Ianjamasimanana R., Hammer F., Higgs C., Namumba B., Carignan C., Józsa G. I. G., McConnachie A. W., 2022, arXiv e-prints, p. arXiv:2204.03662
- Zhang H., Zaritsky D., 2022, arXiv e-prints, p. arXiv:2210.10043

## APPENDIX A: RAM PRESSURE METRICS

This paper has been typeset from a TeX/LaTeX file prepared by the author.

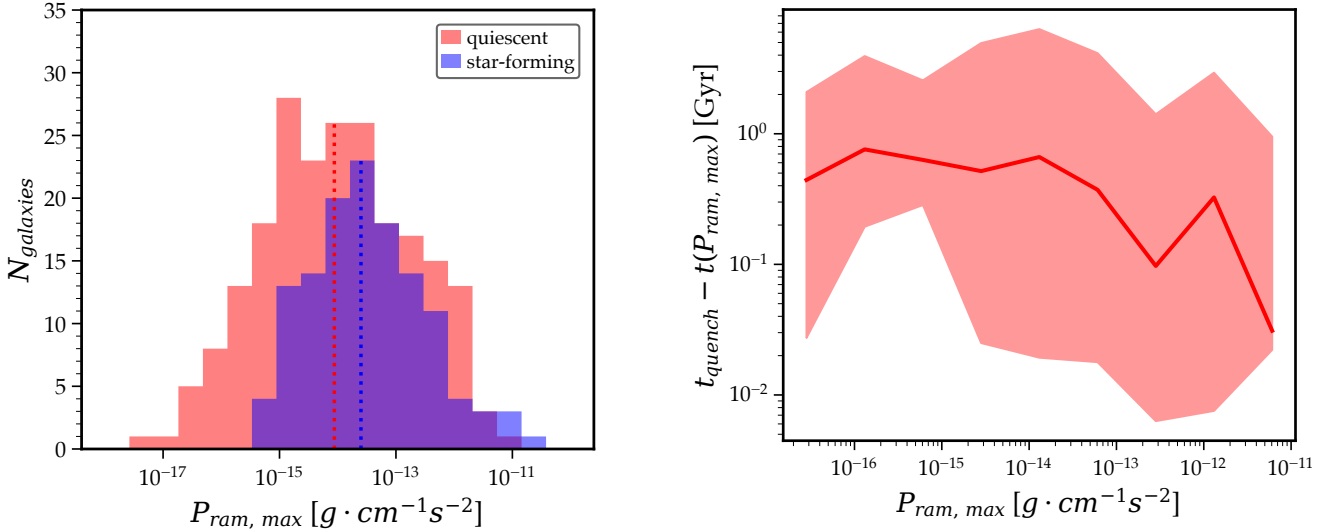


**Figure A1.** Same as Figure 6, but the x axes are  $P_{\text{ram}, \text{max}}$ . The quiescent and star-forming populations do not have significantly different characteristic values of  $P_{\text{ram}, \text{max}}$ , and  $P_{\text{ram}, \text{max}}$  does not correlate as much with quenching delay time compared to  $R_{\text{max/int}}$ .

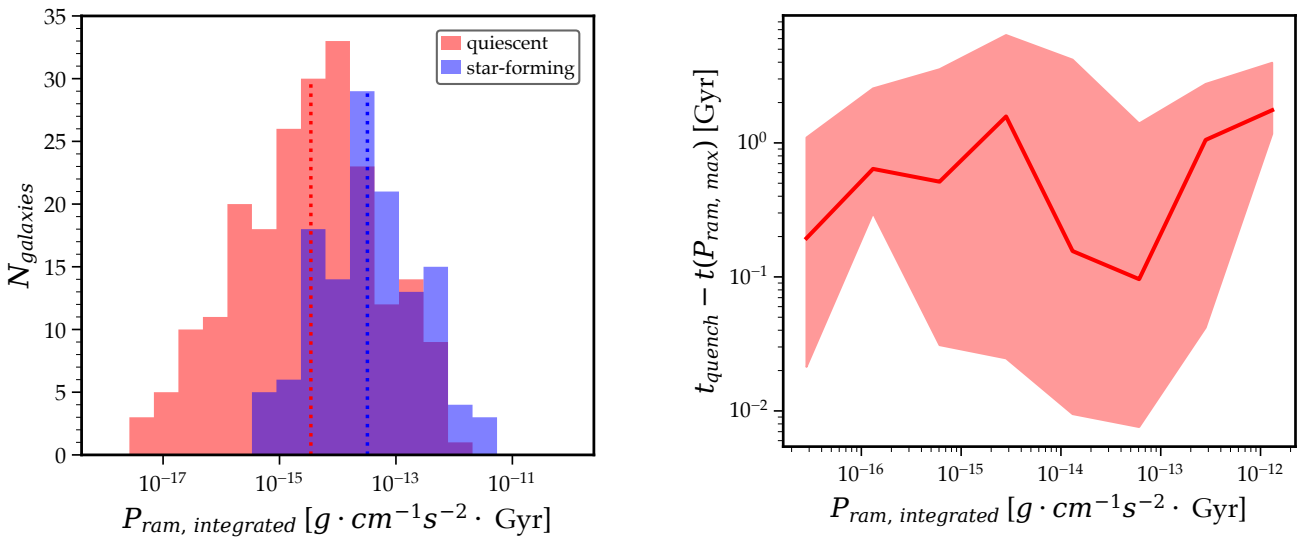


**Figure A2.** Same as Figure 6, but the x axes are  $P_{\text{ram}, \text{integrated}}$ . The quiescent population has slightly lower characteristic values of  $P_{\text{ram}, \text{integrated}}$ , and  $P_{\text{ram}, \text{integrated}}$  does not correlate with quenching delay time compared to  $R_{\text{max/int}}$ .